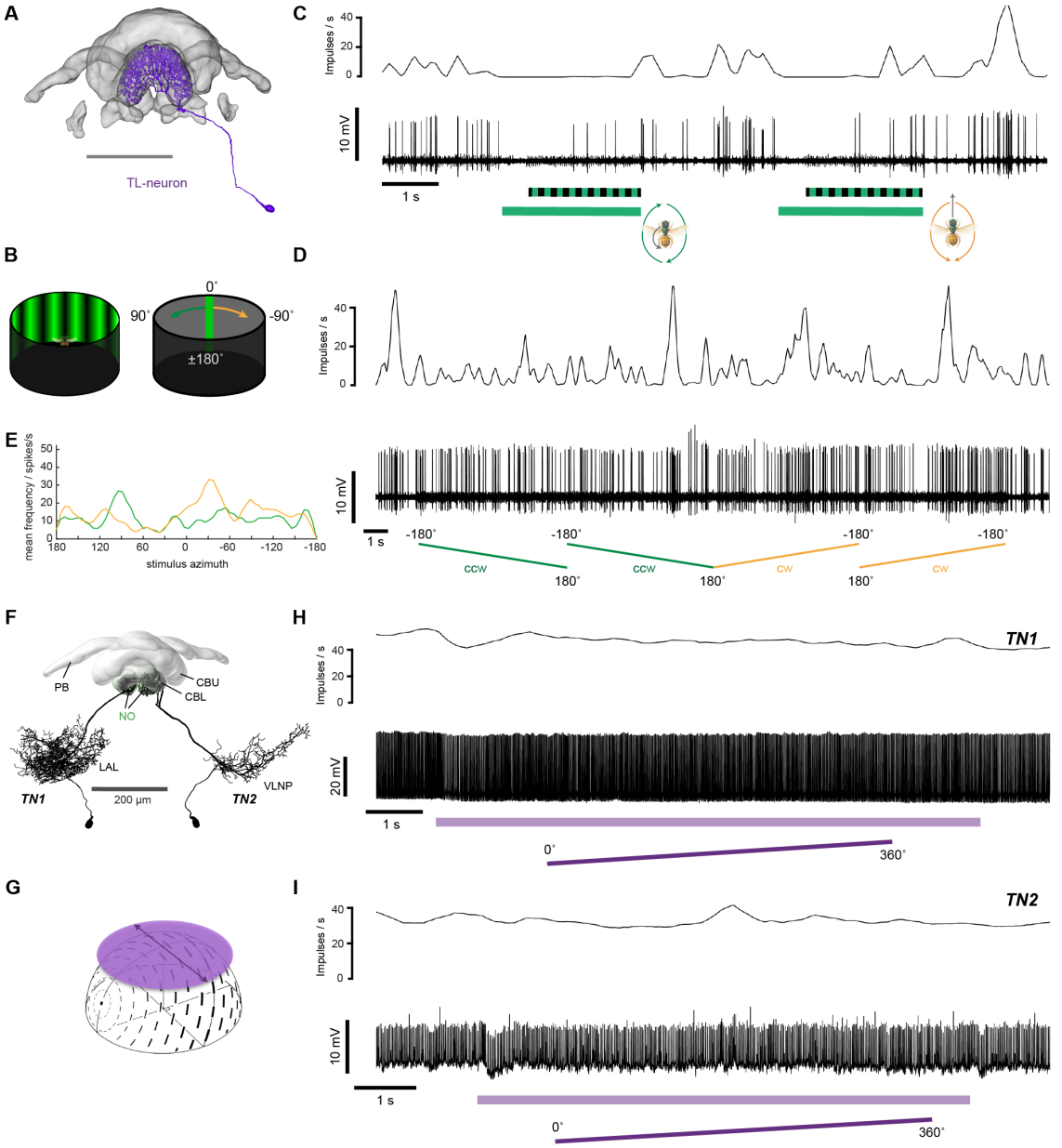

Figure S1. Neural responses to polarized light in speed neurons and optic flow in compass neurons; Related to Figures 1, 2 and 3.

(A). Anatomy of 'compass neuron' (TL-neuron) of *Megalopta genalis*. (B). Illustration of stimuli shown to the bee in C-E. Left: Full-panorama optic flow stimuli shown in LED arena (used to obtain results in C). Right: Receptive field mapping via bright bar moving around the bee clockwise (cw) and counter-clockwise (ccw) (used to obtain results in D,E). (C). Typical response (bottom: spike train; top gliding average activity) to short bouts of optic flow stimuli in compass neurons. Shown were both translational optic flow (stimulated forward flight; 60˚/s) and rotational optic flow (cw; 60˚/s). Lights on is indicated by the green bar, while duration of motion is indicated by the dashed line. Both stimuli elicit a weak, transient inhibition at the onset of the stimulus display (before motion begins). These stimuli were tested in 5 out of the 10 recordings of

compass cells. Four cells yielded responses highly similar to the one shown, while one cell responded with weak transient excitation at motion onset. (D). Neural response (as in C) to a bright bar moving around the bee at 60˚/s. Ramps indicate duration and direction of bar movement. No consistent response is visible during ccw turns, while cw turns lead to a weak inhibition followed by an excitation in both consecutive rotations, but the response amplitude does not exceed background variability. (E). Plot of activity shown in D against azimuth of the bar in the arena. Colors indicate cw and ccw turns (shown is average of two rotations). This stimulus was shown in 9 out of 10 compass cell recordings and let to either no response or to weak, inconsistent responses similar to the one in D/E. (F). Anatomy of speed neurons (TN-cells). For details see Figure 2. (G). Schematic illustration of polarized-light stimulus used to obtain results in H,I. The dorsally placed filter was rotated at 60˚/s and illuminated by UV LEDs. (H,I). Neural responses to a rotation of the polarizer (as in Figure 1) in a TN1 (H) and a TN2 neuron (I). Purple bar: lights on duration. Purple ramp: filter rotation. No response to the E-vector orientation is detectable. A weak transient inhibition occurs at lights on. This stimulus was tested in 5 out of 14 recordings of speed neurons (3 out of 9 TN1 cells, and 2 out of 5 TN2 cells). Related to Figure 1.

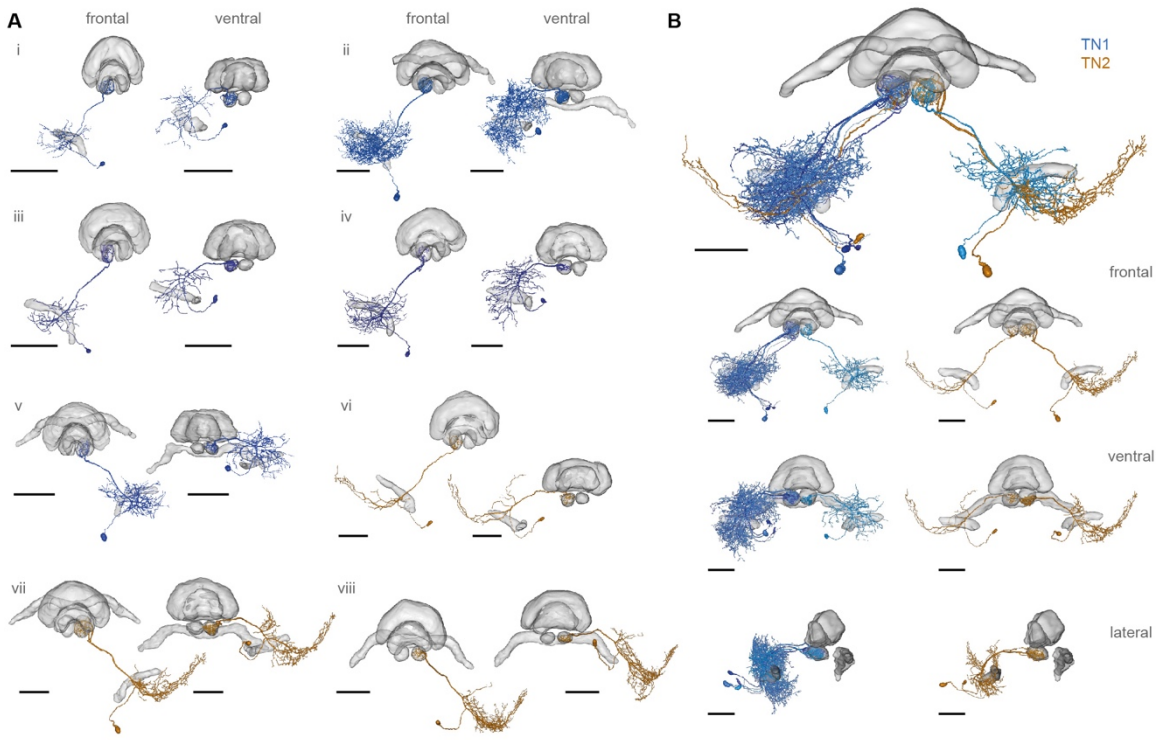

Figure S2. Morphology of TN1 and TN2 neurons; Related to Figure 3.

(A) 3D-reconstructions of TN1 neurons (i-v) and TN2 neurons (vi-viii) from *Megalopta* bees (i-vii) and bumblebees (viii) shown together with reconstruction of the central-complex neuropils and the lateral antennal-lobe tract (lALT) for better orientation. Left panels: frontal views; Right panels: ventral views. (B) All *Megalopta* neurons from (A) affinely registered into a common reference brain, TN1 cells in blue, TN2 cells in orange. Bottom rows: TN1 and TN2 cells shown separately from frontal, ventral and lateral views to illustrate the different shapes of arborizations between the two cell types, as well as their highly consistent arborizations within each cell type. Note that both cell types overlap in one small region ventral of the lALT. Please also refer to Movie S1 as well as www.insectbraindb.org for additional visualization of the neurons. Scale bars: 100 µm. Related to Figure 3.

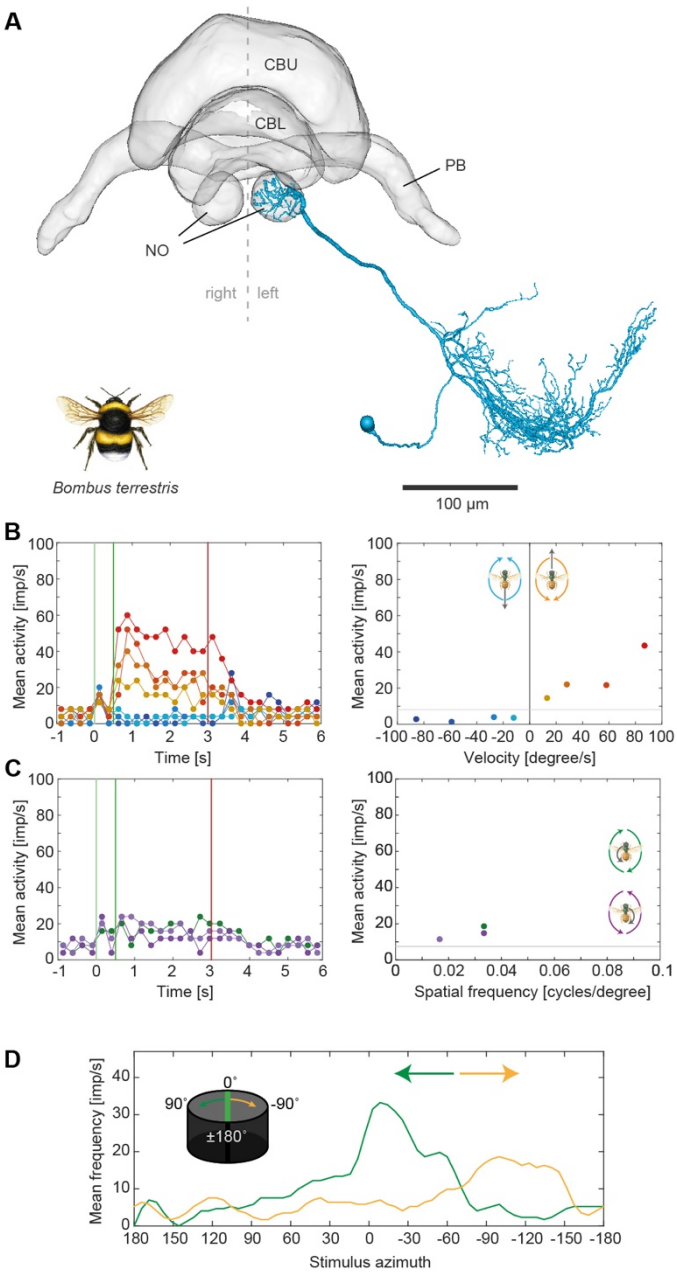

Figure S3. Physiology and anatomy of a bumblebee speed neuron; Related to Figures 2,3.
(A) 3D reconstruction of a bumblebee TN2 cell (homologous to *Megalopta* TN2 cell from Figure 3). CBU, upper division of the central body; CBL, lower division of the central body; PB, protocerebral bridge; NO, noduli. (B) Responses to different velocities of translational optic flow (blue: back to front; orange: front to back). Left: mean frequency during stimulation bouts (0.25 s bins); right: mean frequency during the last 2 s of each stimulation plotted against movement speed. (C) As in (B), but data for different spatial frequencies of clockwise (green) and counter-clockwise (purple) rotational optic flow. Note that only three data points could be obtained during this stimulus presentation. (D) Receptive field of the same cell type. Yellow trace: Response to a green bar moving around the bee clockwise. Green trace: counter-clockwise movement. In summary, all stimulus responses are highly similar to the ones from *Megalopta* presented in Figures 2,3 and indicate conservation of both structure and function of the presented neural circuit. Related to Figures 2,3.

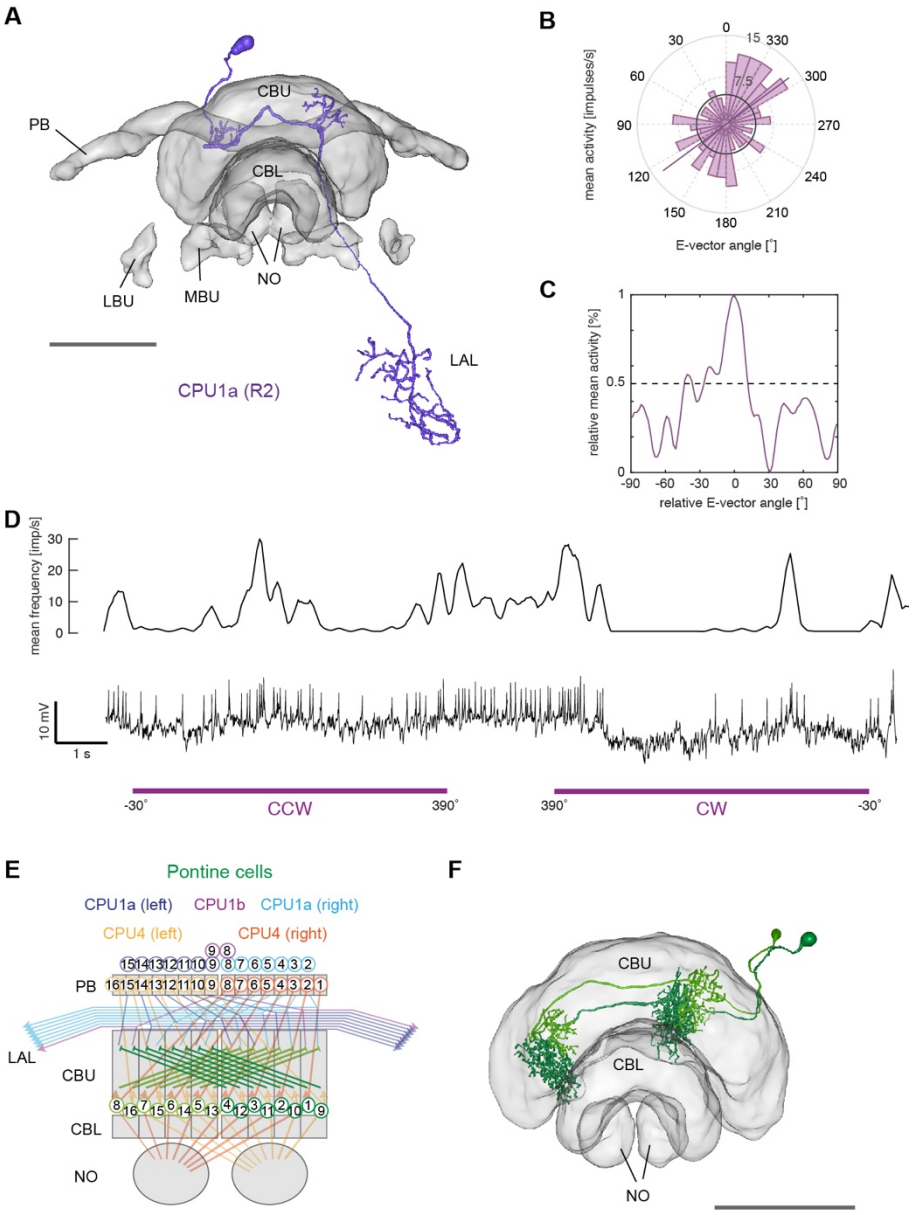

Figure S4. Anatomy and Physiology of *Megalopta* CPU1 and anatomy of pontine neurons; Related to Figures 1,5.

(A) 3D reconstruction of CPU1 neuron shown with 3D surface reconstruction of surrounding neuropils. (B) Average response of the cell in (A) to a rotating polarizer (2 clockwise (CW) and 2 counter clockwise (CCW) rotations). Black circle: background activity; Purple line: mean tuning angle. (C) Tuning width of the same cell (as in Fig. 1H). (D) Raw spike train of the same cell. Top trace: gliding average mean activity; bottom trace: spike train. Consistent with data from locusts, monarch butterflies, and dung beetles these responses are much noisier compared to input-stage compass neurons (Figure 1) , which is, in fact, predicted by our model for our experimental situation, in which the state of the second main input, the CPU4 cells, is not experimentally controlled. (E) Connectivity scheme of pontine neurons required to balance memory between right and left brain hemispheres. (F) Two examples of pontine cells from *Megalopta*, shown as 3D reconstructions together with the structures of the central complex (grey). Abbreviations: PB, protocerebral bridge; CBU, upper division of the central body; CBL, lower division of the central body; NO, noduli; LAL, lateral accessory lobe; LBU lateral bulb; MBU, medial bulb. Scale bars: 100 µm. Related to Figures 1,5.

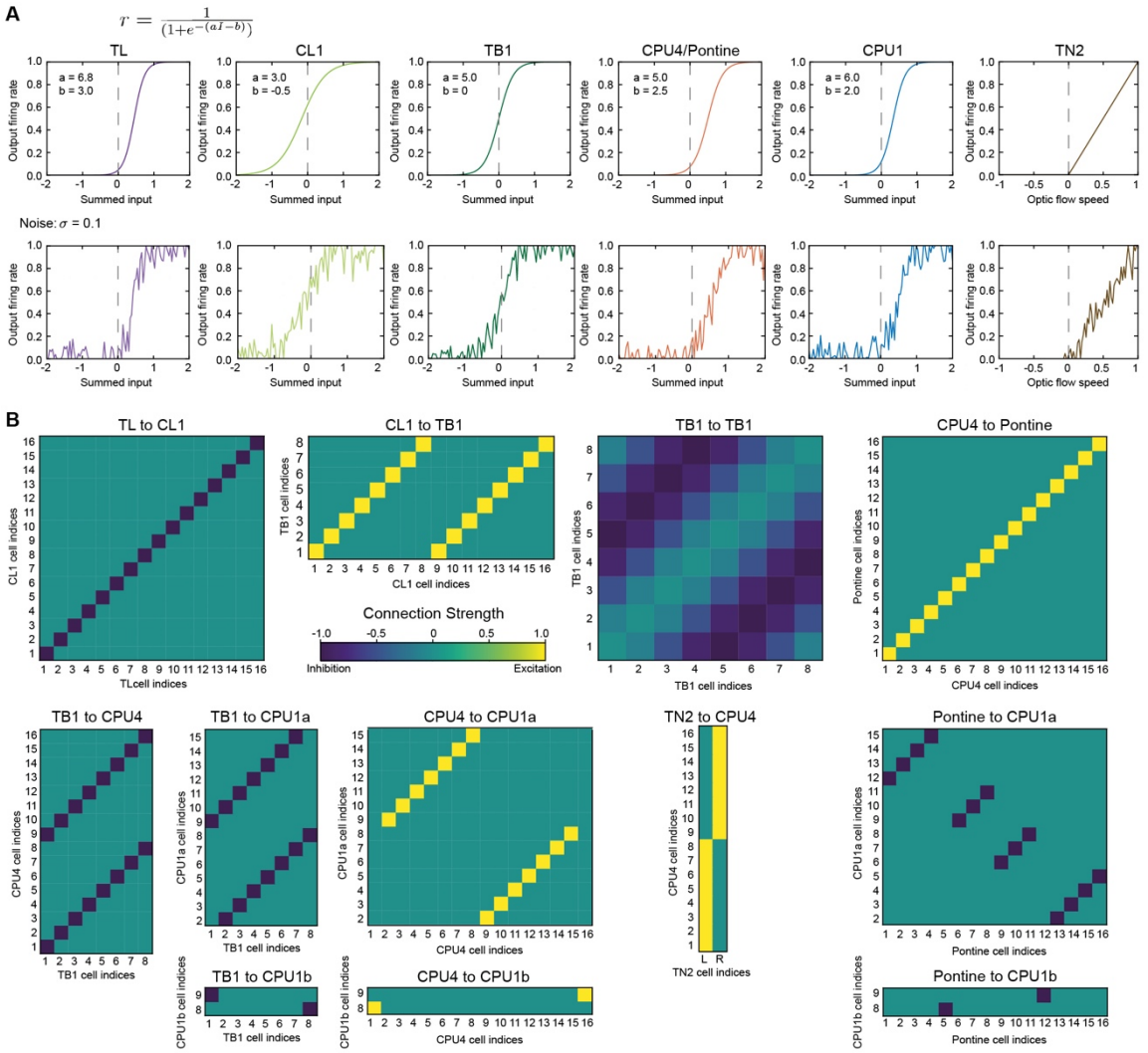

Figure S5. Connectivity and model parameters of the components of the path integration circuit; Related to Figure 5.

(A) Top: equation used to compute output from summed input of neurons. Parameters a and b were tuned to generate different neuron types. Resulting shapes of sigmoids for each neuron type without added noise (top row) and with 10% added noise (bottom row); parameters a and b are shown. Pontine cells and CPU4 cells have identical sigmoid parameters. (B) Connectivity matrices between all cell types used in the circuit. Cells were either fully inhibitory or fully excitatory (synaptic strengths were not tuned), except mutually inhibitory interconnections between TB1 neurons, which formed a sinusoidal weight matrix crucial for the resulting ring-attractor network. Related to Figure 5.

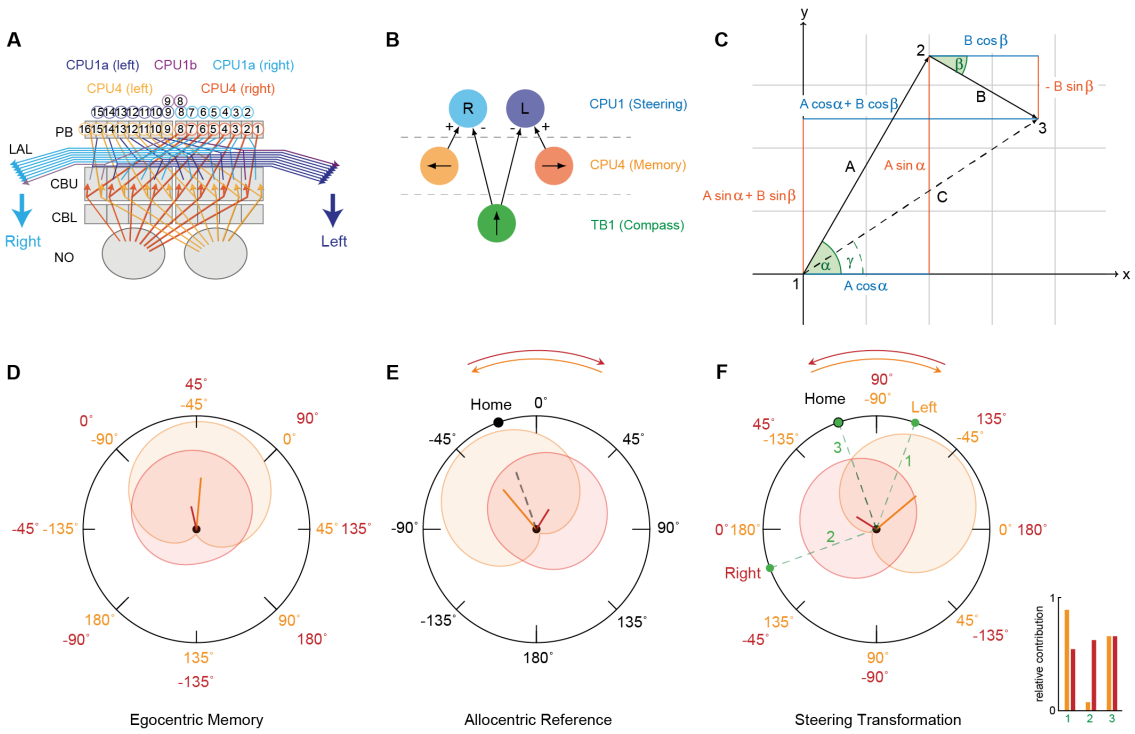

Figure S6. Mathematical explanation of memory and steering components of model; Related to Figure 5.

(A) Schematic connectivity between CPU4 (memory) and CPU1 (steering) neurons. Memory is charged relative to TN excitation proportionate to translatory motion along their preferred angle of expansion for optic flow, so each CPU4 column is effectively storing motion at a ±45° offset from their TB1 (compass) input preference angle. An additional columnar offset between CPU1 and CPU4 means that each steering cell receives input from TB1 and CPU4 at ±90° offsets. (B) A segment of the circuit (Figure 5E) illustrates how it gives rise to homing. When facing downwards the TB1 neuron (green) is minimally excited. The CPU4 columns representing home vector to the left and the right of the downwards direction (orange) are effectively compared. The memory that evokes the highest output will drive steering in that direction by exciting CPU1 cells (blue). (C) Motion can be described using polar coordinates, which in turn can be expressed as a sinusoid. Successive motion from points 1 to 2 and 2 to 3 could be represented by two sinusoids with phase α and β and amplitude A and B. Summing them results in another sinusoid representing the motion from 1 to 3 with phase γ and amplitude C. (D-F) Homing can be described by comparison of two populations of CPU4, forming a compound memory to store a sinusoidal home vector. (D) When aligning the activity bumps by actual CPU4 columns, each population stores motion at a ±45° offset. (E) For visualization purposes, when rotated the sinusoids sum to give the home vector (dashed grey line). (F) The connectivity columnar offset to CPU1 shifts by an additional ±45°, allowing populations to be compared to determine left or right turning. Facing towards direction 1 (green line) the agent turns left as activity from the light orange population dominates. When facing towards direction 2 the agent turns right. Finally, when facing to direction 3 the agent will keep going straight as both population activities balance. If facing directly away from home, the noise in the system breaks the symmetry, causing the agent to turn in either direction. Inset: Activation ratio of right and left memory for the three directions. Related to Figure 5.

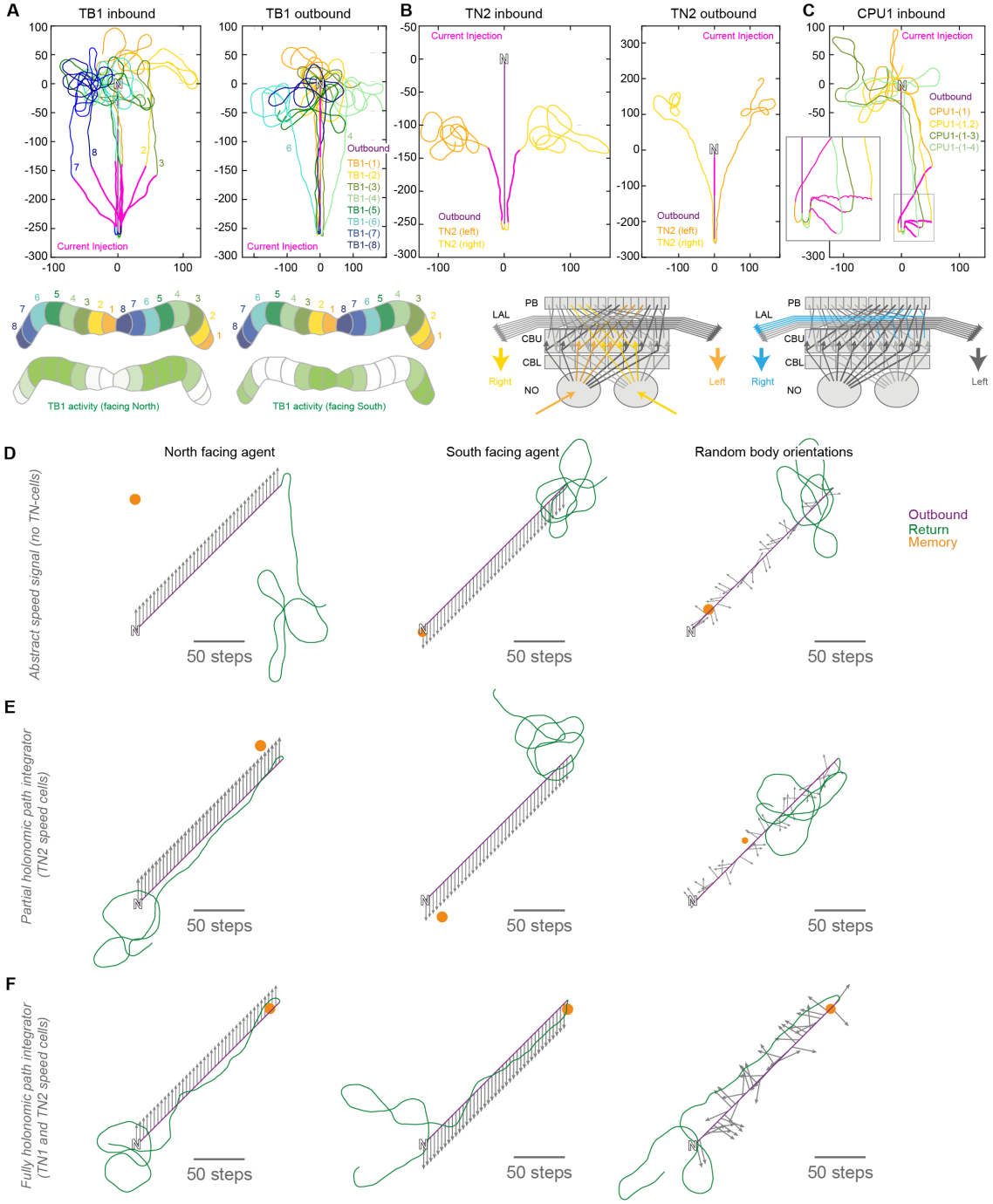

Figure S7. Predictions of the model for physiological and behavioral experiments; Related to Figure 6. (A-C) Virtual current injections into components of the path integration circuit predict specific effects on homing routes in real bees. Injections were either performed during outbound or inbound trips (highlighted as red traces) by clamping the activity of a cell to their maximum firing rate for a fixed period (200 time steps). (A) Injections into TB1 neurons during distinct directional movements cause directional shift in homing vector. Which injections are most effective depends on the location of the injected neuron relative to the peak of the compass activity bump in the PB (bottom schematic traces). As the circuit is not actively

steering during the outbound trip, the injections generate false memories that manifest during homing. (B) Injections into the speed neurons lead to partial unbalancing of right and left memory and to directional deviations during homing. Effects are opposite for southwards and northwards facing agent. Schematic below traces illustrates, in principle, which neurons are affected. (C) Effects of directly injecting the steering neurons (single or several CPU1 neurons) during the homing phase, when the circuit is actively steering. The agent deviates from its homing direction in a predictable direction by an angle correlated to the number of injected neurons. The inset highlights characteristic spiraling, increasing upon injection of more than one CPU1 cell. (D-F) Results of outbound routes with specific, optic-flow induced mismatches of body angle (grey arrows) and flight direction for a model without speed neurons, i.e. containing an abstract speed signal (D), the partly holonomic model used for the results in this paper (E), and a fully holonomic model, which incorporates all identified speed neurons, but requires several additional assumptions (see supplementary experimental procedures below). (F). Right panels: optic flow direction changes randomly every 25 steps and leads to different predictions for each model. The orange dots indicate the position estimate based on the readout of CPU4-neuron activity. Related to Figure 6.